Original Research

Mitterfels

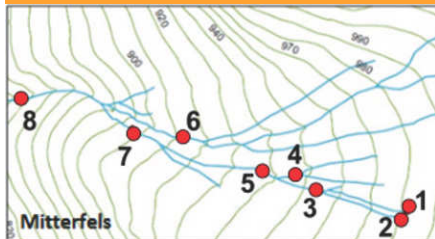### Core Ideas

- There are three distinct fractions of natural nanoparticles and colloids.
- These unique fractions have different preferential P binding.
- The fractions include Fe–P, organic C–P, and clay–P.
- Field flow fractionation coupled online to OC detector for size resolved OC detection.

N. Gottselig, W. Amelung, R. Bol, H. Vereecken and E. Klumpp, Institute of Bio- and Geosciences, Agrosphere (IBG-3), Research Center Jülich GmbH, Jülich, Germany; V. Nischwitz, Central Institute for Engineering, Electronics and Analytics, Analytics (ZEA-3), Research Center Jülich GmbH, Jülich, Germany; T. Meyn and C. Halle, Dep. of Hydraulic and Environmental Engineering, Norwegian Univ. of Science and Technology, Trondheim, Norway; W. Amelung and J. Siemens, INRES Soil Science and Soil Ecology, Univ. of Bonn, Bonn, Germany; J. Siemens, Institute of Soil Science and Soil Conservation, Justus Liebig Univ. Giessen, Giessen, Germany. *Corresponding author (n.gottselig@fz-juelich.de).

Phosphorus Binding to Nanoparticles and Colloids in Forest Stream Waters

Nina Gottselig,* Volker Nischwitz, Thomas Meyn, Wulf Amelung, Roland Bol, Cynthia Halle, Harry Vereecken, Jan Siemens, and Erwin Klumpp

Elemental contents in catchment headwaters are indicative of the load of nutrients and minerals cycled or released from ecosystems, yet little is known about natural colloids (1–1000 nm) and especially natural nanoparticles (NNP, 1–100 nm) as nutrient carriers in forested headwater streams. We hypothesize that the majority of P is bound to NNP in forest streams but that their size and composition varies for different forested headwater systems. Four forested sites in Germany and one in Norway, which differ in total P content, were sampled for stream water and analyzed for colloids. The samples were fractionated using field flow fractionation coupled to inductively coupled plasma–mass spectrometry and an organic C detector. The results showed that NNP and colloids from all sites could be separated into three distinct fractions (approximately 1–20 nm, >20–60 nm, and >60 nm). The elemental concentrations of P, organic C, Al, Si, Fe, and Mn in the fractions differed among the five sites. However, cluster analysis showed that each fraction had unique elemental signatures with different preferential P binding partners. Phosphorus was preferentially associated with Fe in the smallest size fraction, with an increasing contribution of organic-C-associated P as the fraction size increased. The largest fraction was dominated by clay minerals. Also, the data indicated that the relative contribution of the NNP and colloidal fractions for ecosystem nutrient supply rises as total P concentrations decline. The study highlighted the still underestimated importance of NNP for matter transport in forest streams and thus P cycling.

Abbreviations: AF^4, asymmetric flow field flow fractionation; FFF, field flow fractionation; ICP–MS, inductively coupled plasma–mass spectrometry; NNP, natural nanoparticles; OCD, organic carbon detector; UV, ultraviolet.

Colloids (1–1000 nm) in stream water samples have the potential to act as predominant carriers of elements in ecosystems (Wilkinson et al., 1997; Binkley et al., 2004; Filella et al., 2006; Qafoku, 2010; Stolpe et al., 2010; Liu et al., 2011; Gottselig et al., 2014). As a subset of colloids, natural nanoparticles (NNP) are uniquely specified in the size range of 1 to 100 nm (Qafoku, 2010; Hartland et al., 2013) due to their larger specific surface area and thus increased reactivity (Qafoku, 2010; Hartland et al., 2013) in comparison to larger sized colloids (>100–1000 nm). This definition of nanoparticulate and colloidal size ranges thus overlaps with the definition of dissolved components (Martin et al., 1995; Hill and Aplin, 2001; Jarvie et al., 2012), which are operationally defined as the fraction passing a 450-nm filter (Greenberg, 1985; Binkley et al., 2004; Regelink et al., 2013). Several studies have already shown that these fractions are also relevant for major nutrients such as P, which is not only present in dissolved P forms in stream waters but also bound in or on colloids in significant amounts (Martin et al., 1995; Mayer and Jarrell, 1995; Stolpe et al., 2010). Fine P-carrying colloids have also been detected in soil solution (Owens and Shipitalo, 2006; Jiang et al., 2015) and forest surface waters (Gottselig et al., 2014). Natural nanoparticles and colloids may thus also control the transport and availability of P in aqueous phases (Heathwaite and Dils, 2000; Montalvo et al., 2015).

Elemental concentrations in forested headwater catchments result from both nutrient cycling and nutrient release processes in forest ecosystems. The nutrient load exported with headwaters represents a baseline for downstream water quality and nutrient cycling. Due to the acidic conditions, especially below coniferous forests, in forest soils and thus stream waters, a high adsorption of ions and molecules to particle surfaces can take place (Franco et al., 2009; Crini and Badot, 2010). Under these pH conditions, P is rapidly complexed with Fe and Al compounds (Reddy et al., 1995) while surfaces of metal (hydr)oxides are positively charged, thus acting as adsorbents for anions and organic matter. In rivers with catchments dominated by silicate rocks and low pH values, Ca-rich particles as another potential P carrier are less relevant (Hill and Aplin, 2001). According to Gottselig et al. (2014), the mean portion of P bound to NNP and colloids in forest stream waters varies between 3 and 100% depending on the source and composition of the tributary flow. More precisely, only tributaries strongly influenced by groundwater flow exhibit low percentages (3%), whereas mean portions of all other investigated tributaries (e.g., those dominated by surface waters) exceed 40% of total P.

In general, aquatic NNP and colloids can be rich both in minerals, with which P associates, or organic matter containing significant amounts of organically bound P (Darch et al., 2014). Clay minerals, specifically, can strongly adsorb phosphate (Edzwald et al., 1976) or act as carriers for P through ligand exchange of phosphate with metal hydroxides on the exchange surface (Yaghi and Hartikainen, 2013). All colloidal constituents are either present as these single components (minerals or organic) that can associate with P species, or can form organomineral complexes (Klitzke and Lang, 2007, and references therein). Additionally, organic matter can act as a polymer that stabilizes colloids (Ranville and Macalady, 1997) so that they are less prone to aggregate to larger size ranges. First studies on the size-resolved analysis of NNP and colloids (e.g., Hassellöv et al., 1999; Lyvén et al., 2003; Dahlqvist et al., 2004; Stolpe et al., 2005, 2010; Andersson et al., 2006; Neubauer et al., 2013; Regelink et al., 2013, 2014; Gottselig et al., 2014) showed the importance of colloidal components such as minerals, metal oxides, or organic molecules, which can be building block structures of NNP and colloids. These components additionally vary depending on the NNP and colloid size. It is still disputed whether Fe and Al, both in ionic and oxide forms, are relevant especially for small NNP (<20 nm) in the context of associated P transport (Francko and Heath, 1982; Richardson, 1985; Leppard et al., 1988; Hassellöv and von der Kammer, 2008; Jiang et al., 2015) or if organic matter transports P in the smallest size fraction (Shafer et al., 1997; Lyvén et al., 2003; Regelink et al., 2011, 2013). This disagreement over the preferential binding partners of P in the different size fractions is due to the fact that the statements about P speciation are made on account of the maximum likelihood of P binding in the fractions, yet they need further validation through the application of exploratory data analysis techniques.

In contrast to methods used in earlier studies on environmental colloids, field flow fractionation (FFF) (Giddings et al., 1976) provides a size-resolved analysis of the NNP and colloidal fractions. It is a flexible technique for nearly nondestructive fractionation of colloidal and especially nanoparticulate samples (Gimbert et al., 2003) without the need for sample pretreatment, i.e., is best suited to characterize the size distribution of NNP and colloids in the aqueous environment. The separation of particle fractions occurs primarily due to the hydrodynamic particle diameter but also partially to morphology and the particle electrostatic properties and is driven by an interaction between the strength of the applied separation field and the diffusion coefficient of the colloids (Baalousha et al., 2011). To determine the elemental composition of NNP and colloids, inductively coupled plasma–mass spectrometry (ICP–MS) is a powerful online detector for the FFF (e.g., Nischwitz and Goenaga-Infante, 2012). Important studies on the application of FFF–ICP–MS on urban stream water NNP and colloids (Hassellöv et al., 1999; Lyvén et al., 2003; Stolpe et al., 2005) as well as on forested stream water NNP and colloids (Dahlqvist et al., 2004; Andersson et al., 2006) have been published, yet the role of colloids in stream waters is still less understood. The applied FFF–ICP–MS method is applicable to routine analysis and detects low P concentrations through the use of the collision cell technology (Gottselig et al., 2014). In addition to ICP–MS, it is possible to use an organic C detector (OCD) coupled to FFF. It overcomes the compound-dependent response for C in ultraviolet (UV) detection, for example failing to detect organic acids (Reszat and Hendry, 2005). Further, a separation of the NNP and colloids from the truly dissolved phase (<1 kDa) is achieved through the specific technique of flow field flow fractionation because the truly dissolved phase passes the separation membrane of the channel, thus allowing a clearer distinction among NNP, colloids, and truly dissolved species (Martin et al., 1995). It should be noted that through FFF–ICP–MS coupling, no information on the speciation of P (Spivakov et al., 2009) is gained apart from the particle size.

The objective of this work was to test the hypothesis that the majority of P is bound to NNP in forest streams but that the size and elemental composition varies for different forested headwater systems. This work was conducted as a follow-up, extension, and enhancement of the study on variable tributary and main stream flows within one catchment (Gottselig et al., 2014). Hence, base flow events of stream waters and tributaries in forest catchments of Germany and Norway were sampled in the current study. The sites differed in total P load and therefore potentially also in the distribution of P among NNP and colloidal size fractions. The samples were analyzed using FFF coupled to ICP–MS and to an online high-sensitivity OCD.

Materials and Methods

Sampling Sites and Stream Points

Four forested sites in Germany (Fig. 1), three of which are Level II sites (defines specific methods applied to long-term forest observation sites, http://www.forstliche-umweltkontrolle-bb.de) of the Intensive Long Term Monitoring Network of Forest Ecosystems across Europe that are investigated in the framework of the DFG priority program 1685, and one that is a Terrestrial Environmental Observatories (TERENO) experimental test site in the Eifel/Lower Rhine Valley Observatory, were sampled. The Level II sites are Vessertal in Thuringia, Mitterfels in Bavaria, and Conventwald in Baden-Württemberg; the TERENO site is Wüstebach in North Rhine-Westphalia. The latter site experienced a clear-cut of one-third of the area in late 2013.

For comparison and to increase the studied range of environmental and climatic conditions, a forested site in Norway was additionally sampled. This site is Leirelva in Sør-Trøndelag (Fig. 1). In contrast to Germany, Norwegian streams originate mainly from surface water because solid bedrock starts quickly below the thin soil layers. Further, it was observed for Norway that there has been an increase in forest stocks since 1990 (Liski et al., 2002), so that C and associated P inputs into streams with near-surface runoff might increase as well.

All analyzed sites are forested, with acidic soil and stream water pH values. The German Level II sites are dominated by beech trees and the Norwegian site is dominated by spruce trees. Bedrock types are shales with occasional sandstone inclusions (Wüstebach), gneiss (Mitterfels, Conventwald, and Leirelva), and trachyandesite (Vessertal). Mean annual temperatures are 5.5°C (Vessertal), 4.5°C (Mitterfels), 6.8°C (Conventwald), and 5.0°C (Leirelva). The total annual precipitation is 1200 L m^{-2} in Vessertal (1995–2003), 1299 L m^{-2} in Mitterfels (1991–2009), 1749 L m^{-2} in Conventwald (1997–2005) (Jaane Krüger, personal communication, 2015), and 857 L m^{-2} in Leirelva (Climatemps, 2014).

Sampling was performed in Vessertal at five stream points, in Mitterfels at eight stream points, in Conventwald at five stream points, in Wüstebach at seven stream points, and in Leirelva at four stream points. The 29 stream points were chosen according to the findings of Gottselig et al. (2014) to reflect tributary flow, main stream flow, and inflow from differing hydromorphological areas of all sampled streams.

Sampling and Sample Preparation

Base flow stream water samples were collected in mid-August 2014 from all sampling sites. Due to analytical constraints, only one point in time could be selected. At sampling, electrical conductivity at the catchment outlet points was 39.9 µS cm^{-1} in Vessertal, 21.2 µS cm^{-1} in Mitterfels, 36.5 µS cm^{-1} in Conventwald, 159.0 µS cm^{-1} in Wüstebach, and 119.2 µS cm^{-1} in Leirelva. Stream water pH values ranged between 5.8 (Wüstebach) and 6.8 (Leirelva), and stream water temperature between 12.4°C (Mitterfels) and 14.9°C (Leirelva) (Supplemental Table S1).

Samples were stored cool at 4°C in polytetrafluoroethylene bottles, and analysis was started within 1 wk after sampling. Prior to analysis, the stream water was homogenized by shaking and a volume of 15 mL was filtered through prerinsed 5-µm cellulose nitrate filters (GE Healthcare) to avoid potential clogging effects of the filter and of the narrow FFF tubing. These 15-mL samples were used
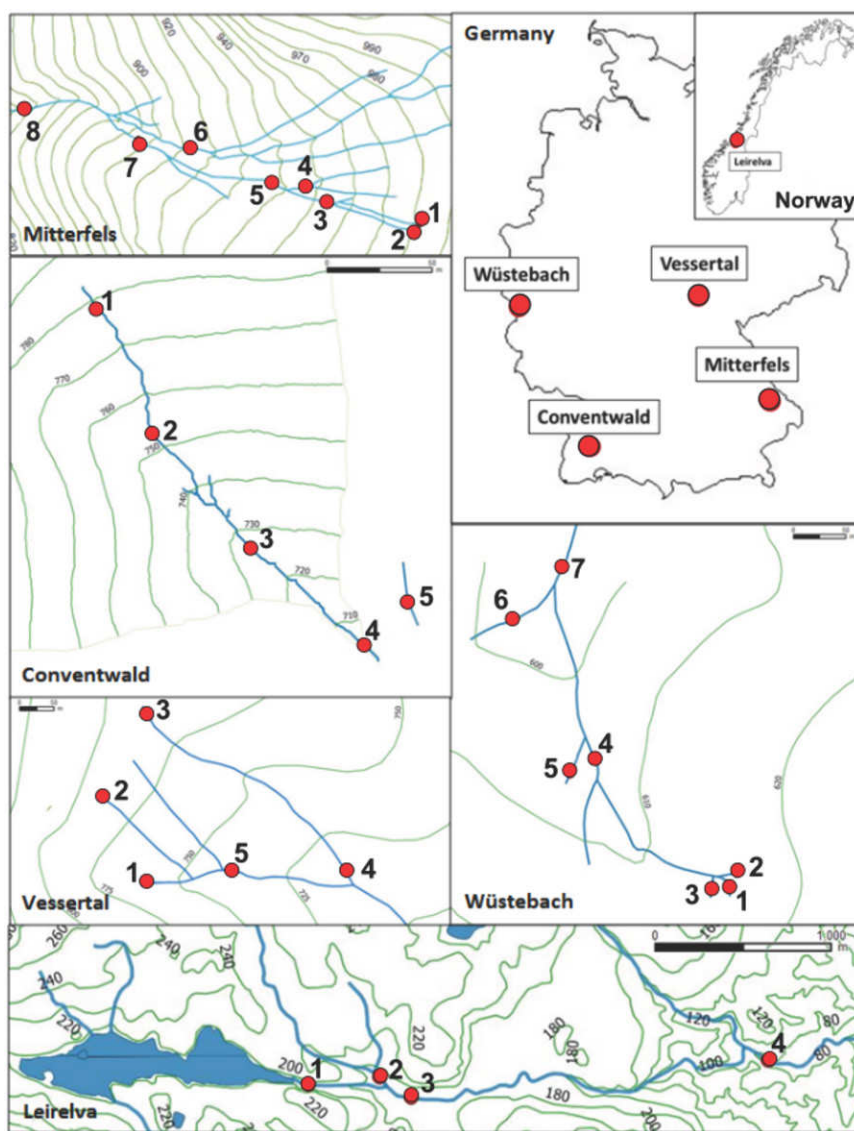

Fig. 1. Map of sampling sites. Maps are oriented to the north. Scale bars except Leirelva represent 50 m; Leirelva scale bar shows 1000 m.

for FFF fractionation coupled to ICP–MS and to OCD and for measurement of total elemental concentrations with ICP–MS and OCD. Filtration at more commonly known cutoffs was purposely not conducted because it has been shown that membrane clogging occurs when filtering close to target size ranges of the analytes, which would have resulted in a severe risk of underestimating NNP and colloidal concentrations (Zirkler et al., 2012).

Field Flow Fractionation

The nanoparticles and colloids were fractionated with an asymmetric flow field flow fractionation (AF^4; Postnova Analytics). The fractionation method and channel parameters were adapted from Gottselig et al. (2014), but instead of the 10-kDa regenerated cellulose membrane, a 1-kDa polyethersulfone membrane was used for higher resolution of low-nanometer size ranges. For the AF^4 systems, membranes with differing molecular weight cutoffs are available. It is most suitable to use 1 kDa as the cutoff between NNP and truly dissolved species, which corresponds to an equivalent diameter of 0.66 nm (Erickson, 2009, Eq. [2].2). Further, a 500-μm spacer, a 25-μM NaCl eluent, and a cross flow of 3 mL min^{-1} was applied and linearly decreased during the method. Initially, the system was calibrated through a multipoint linear calibration injected at 0 mL min^{-1} cross-flow (Gottselig et al., 2014). Reference materials (Suwanee River NOM, Humic Acid Standard II, and Fulvic Acid Standard II from the International Humic Substances Society; Sulfate Latex Standards 8% w/v 21–60 nm from Postnova Analytics) were used for calibration of the particle diameters included in each size fraction. Elution times of the reference materials are given in Supplemental Fig. S1. The specified diameters of the particles are equivalent sizes to the elution time of the reference materials. A UV detector (254 nm) and the technique of dynamic light scattering (DLS) were also applied for online measurements. The DLS was used to determine especially the size of the largest size fraction (>50 nm). Blank runs inserted between sample runs in the measurement sequence showed no significant peaks.

Online Detection with ICP–MS and Organic Carbon Detection

An AF^4 coupled online to ICP–MS and OCD provides precise and detailed online information by detecting matrix elements including the organic matter contribution within NNP and colloids that are eluting in the same particle size fractions as P and thus are likely to be involved in P binding. For size-resolved detection of particulate Al, Si, P, Mn, and Fe, a quadrupole ICP–MS with collision cell technology (Agilent 7500) was coupled online to the AF^4. Settings for data acquisition from the ICP–MS were used as in Gottselig et al. (2014). For FFF–ICP–MS coupling, a 5-mL sample volume was injected into the AF^4 channel and focused for 30 min. The variation of the ICP–MS peak area for triplicate measurements of a representative sample was calculated to be 5.9% for ^{31}P, 7.6% for [27]Al, 14.0% for [28]Si, 5.3% for [55]Mn, and 15.6% for [56]Fe. The limit of detection was 0.1 μg L^{-1} for P, 0.01 μg L^{-1} for Al, 3.3 μg L^{-1} for

Si, 0.01 μg L^{-1} for Mn, and 0.02 μg L^{-1} for Fe. Using the applied Ar plasma at 1500 W, elemental contents of natural colloids in the size range <300 nm investigated in this study are expected to be fully quantified without the need for digestion prior to introduction into the ICP–MS (Schmitt et al., 2002).

Measurements with an OCD (DOC Labor) coupled online to the AF^4 were also performed. This online organic C measurement nicely complements the spectrum of elements detected online in the NNP and colloidal fractions. The setup and principle of operation of the OCD has been previously described (Huber and Frimmel, 1991; Huber et al., 2011). The OCD system has usually been applied to operationally defined dissolved organic C. Huber et al. (2011) confirmed an oxidation rate of almost 100% for sample constituents below 0.45 μm. The organic C is oxidized in a thin-film reactor and monitored as CO_2 by infrared detection. The resulting C concentration is recorded via the AF^4 software. In general, due to the large volume of the OCD, an offset in the elution time of peaks and a peak broadening can be observed compared with UV and ICP–MS detection. For organic C detection, 1 mL of sample was injected into the AF^4–OCD system. The eluent and the membrane type were the same as described for AF^4–ICP–MS. The fractionation method was also the same with the exception of the focus time, which could be shortened to 10 min due to the smaller injected sample volume. The OCD system was calibrated using dilutions of Certipur liquid organic C standard (EN 1484-H3/DIN 38409-H3, Potassium hydrogen phthalate in water, stabilized, 1000 mg L^{-1}; Merck Millipore 109017) in Millipore water (additionally filtered through 50 nm to remove potential particles in the water) at concentrations of 0.05, 0.1, 0.5, 1.0, 3.0, and 5.0 mg L^{-1}. The same calibration standards were also used for the determination of total organic C in the stream water samples. For this, the AF^4 channel was bypassed by connecting the tip inflow tubing to the detector outlet tubing of the channel. The runtime of the AF^4 method for this data acquisition took 20 min at 0.5 mL min^{-1} tip flow. The relative standard deviation of the organic C concentration for triplicate measurements of a representative sample was calculated to be 2.2%. The limit of detection for organic C was 0.01 mg L^{-1}. Broader peaks were obtained using the OCD than the ICP–MS due to the large volume of the OCD reactor and thus longer sample passage time. Peak integration times for the three fractions were therefore corrected through prolongation of the integration time by 5 min to account for this effect. In general, measurements of total elemental concentration, fraction-specific elemental concentrations, and finally NNP and colloid elemental concentrations expressed as the sum of all three fractions were measured for each element.

Determination of Total Element Concentration

Because the AF^4 technique does not recover dissolved species, total element recovery of aqueous water phases was not assessed in the same run. However, the elemental content of all NNP and colloids

can be related to the total elemental content in the river systems, measured offline without AF[4] fractionation. Total elemental concentrations of P, Fe, Al, Si, and Mn in the filtered, unfractionated samples were determined by quadrupol ICP–MS (Agilent 7500, Agilent Technologies) using external calibration with Rh as the internal standard. Samples were acidified with 1% HCl instead of HNO_3 to avoid mass interference with P by N-containing cluster ions. Collision cell technology with He as the collision gas was applied to minimize spectral interferences.

Data Analysis

The ICP–MS raw data were collected in counts per second (cps) using MassHunter Workstation Software (Agilent Technologies), and OCD raw data were recorded in volts detector signal (V) with the AF[4] analytical software (Postnova). Raw data were exported to Microsoft Excel for peak integration and conversion of peak areas to concentrations through multipoint linear calibration.

For exploratory data analysis, cluster analysis was applied to the quantitative element distribution obtained for the separated particle size fractions to identify fraction-specific preferential binding of P to NNP and colloidal building block elements. Agglomerative cluster analysis with distance measure based on the Pearson correlation coefficient was performed with Statistica for Windows, Version 12.0 (StatSoft Inc.). The results of the cluster analysis are given in distance measures between the elements. These distance measures are given as $1 - $ Pearson r, meaning that the lower the value, the stronger the elements are grouped together. In contrast to statistical significance testing, the cluster analysis uses algorithms that are grouping the parameters with the greatest similarity based on the available samples at the start of analysis. Following this, the threshold regarding the decision when to declare two or more objects to be members of the same cluster is lowered.

All determined elemental concentrations of the particle fractions were transformed to the unit moles per liter prior to data processing and analysis for comparison on the basis of potential binding and substance amounts.

Results and Discussion

Stream Water Natural Nanoparticle and Colloid Fractionation

The data collection from AF[4]–OCD matched well with the respective AF[4]–ICP–MS fractograms (cf. Fig. 2). Both the analyses with ICP–MS and OCD coupled to the AF[4] revealed three fractions of nanoparticles and/or colloids in the samples at the same elution times. An example fractionation depicting the particle fraction peaks, their distinct borders, and the corresponding elemental and organic C concentrations is shown in Fig. 2a and 2b. This represents the dominant occurrence of the measured elements within the three size fractions, despite variations in the

fractionation pattern (= height of the three fraction maxima and width relative to one another) between sites and sampling locations at the sites (see below). Through calibration with reference materials (cf. Supplemental Fig. S1), the first fraction was estimated to include nanoparticles between 1 kDa (membrane molecular weight cutoff) and 20 nm and the second fraction to include nanoparticles >20 to 60 nm. Furthermore, dynamic light scattering revealed that the third fraction included nanoparticles >60 nm to fine colloids up to approximately 300 nm. Due to the fact that no colloids above approximately 300 nm were detected, the entity of colloids referred to in this study is termed *fine colloids*.

The majority of FFF studies with natural aqueous samples have reported two fractions of NNP and colloids in stream waters (Lyvén et al., 2003; Dahlqvist et al., 2004; Stolpe et al., 2005; Andersson et al., 2006; Hassellöv and von der Kammer, 2008), from drainage waters (Regelink et al., 2013), and soil extracts (Regelink et al., 2011, 2014; Jiang et al., 2015). The results of the current study, however, fit well with the FFF findings of Stolpe et al. (2010) and to some extent also Stolpe and Hassellöv (2007), who reported three to four fractions of colloids. The resolution of different peaks of NNP and colloids is primarily a result of the fractionation method applied for FFF, more precisely an interlinked result of membrane type, eluent solution, flow regime, and spacer thickness. It can generally be noted that a greater separation efficiency of the FFF method resolves an increasing number of fractions.

Stream Water Natural Nanoparticle and Colloid Fraction Constituents

Because of multiple elemental peaks within one fraction, first conclusions can be inferred on the chemical speciation of the compounds from reviewing the raw data fractograms (Fig. 2a and 2b). The first of the current three fractions showed narrow high peaks of Fe, organic C, and P (Fig. 2a) as well as Al and UV (Fig. 2b). The second fraction peak was not as narrow as the first and differed in elemental peak intensity compared with the first fraction. Here, Fe (Fig. 2a) and Al (Fig. 2b) show clear peaks, but also organic C, P (Fig. 2a), some Mn, and a UV signal (Fig. 2b) were present. Therefore, the first and second nanoparticle fractions potentially contained P associated with Fe, Al, and organic matter, either with P in association with Fe or Al and Fe- or Al-bound organic C or as P bound to organic C (organophosphorus compounds) that in turn can be bound to Fe or Al. The detected Fe is likely to indicate Fe (hydr)oxides, known to be carriers for P (Mayer and Jarrell, 1995; Stolpe et al., 2010). The third size fraction contained P and all measured elements but in different ratios, with larger amounts of Al and Si (Fig. 2b) than in the first and second fractions. We attribute the presence of Si and Al within the third fraction to clay minerals. Jiang et al. (2015) also showed for an agricultural soil that constituents within one FFF fraction are associated closely with each other and that Fe oxides and organic C may cement nanoparticulate and fine colloidal aggregates that also contain P.
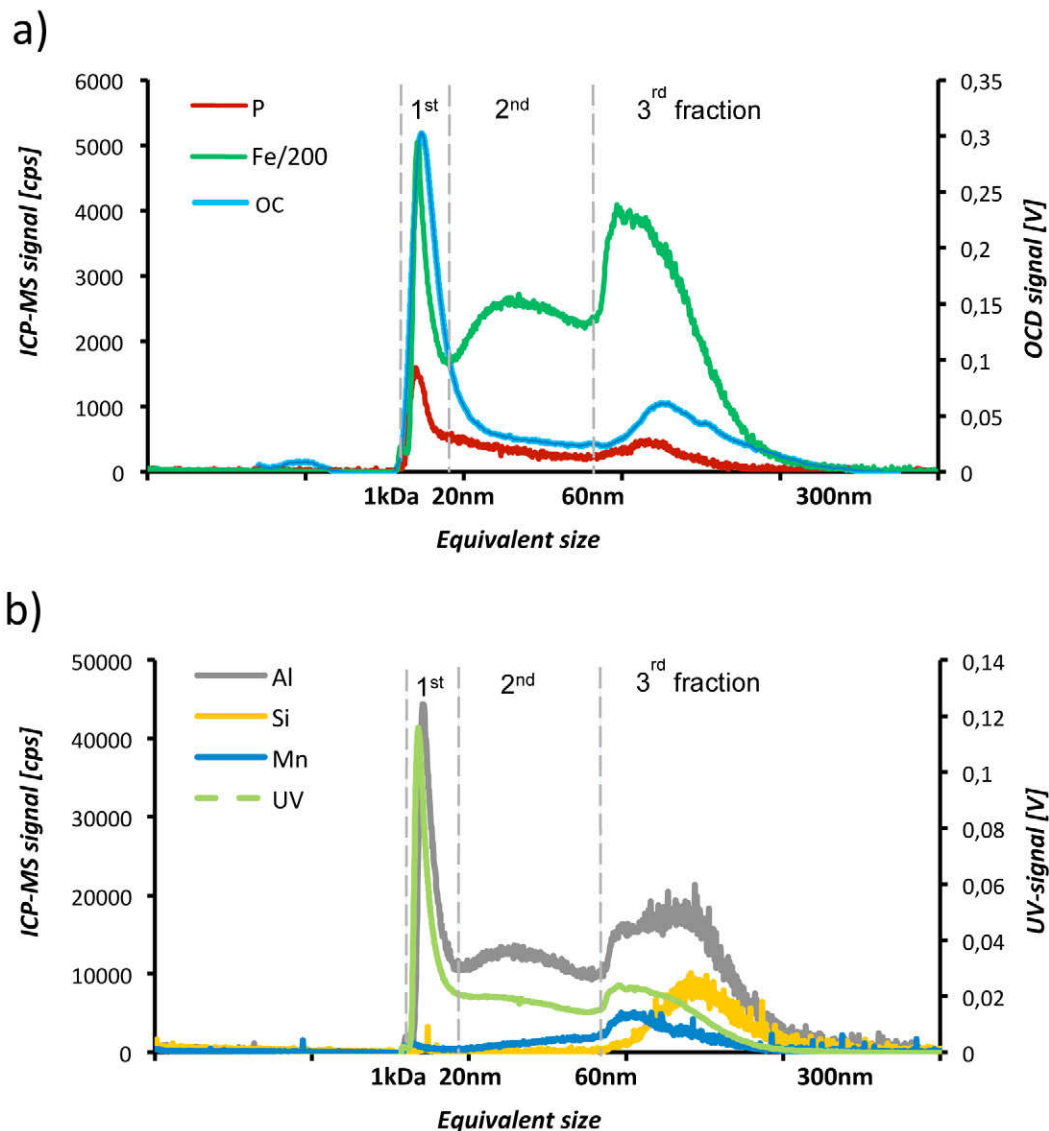
Fig. 2. Example asymmetrical flow field flow fractionation (AF^4) fractograms of Wüstebach Stream Point 7, indicating (a) the three peaks that were detected for all samples: P, Fe, and organic C (OC) signals, with the Fe signal downscaled by a factor of 200 to better visualize the P signal; and (b) Al, Si, Mn, and ultraviolet (UV) signals. The size of the first fraction lies between 1 kDa (0.66 nm) and 20 nm, the second size fraction between >20 and 60 nm, and the third fraction >60 nm. Elution time offset for OC detection (OCD) was corrected, peak broadening was not. The depicted UV signal was recorded at 254-nm wavelength from the AF^4–inductively coupled plasma–mass spectroscopy (ICP–MS) run. Fraction borders apply to the ICP–MS signal; for the OCD evaluation, these borders were modified.

Throughout all the samples, it was evident that P was present in all fractions with varying intensities. The occurrence of Si and Al in the third fraction was characteristic for this fraction and a clear delimitation to the first and second fractions. According to Stolpe et al. (2010), aquatic colloids of the Lower Mississippi River, the Atchafalaya River, the Pearl River, and from marine stations in the northern Gulf of Mexico contain chromophoric organic matter nanoparticles in the size range 0.5 to 4 nm, organic matter nanoparticles with protein-like fluorescence in the size range 3 to 8 nm and >40 nm, as well as Fe-rich colloids in the size range 5 to 40 nm, which all bind P, metals, and Ca. The major components within natural colloids are organic matter and Fe (Hassellöv and von der Kammer, 2008; Neubauer et al., 2013; Darch et al.,

2014; Regelink et al., 2014; Jiang et al., 2015). The present data confirm Fe and organic C as relevant carriers of P next to Si- and Al-containing minerals like clay minerals.

Variability of the Fractionation Patterns of Natural Nanoparticles and Colloids

To assess the on-site and between-site variability of the fractionation patterns of NNP and colloids of forested headwater catchments, the UV absorption at 254 nm (Supplemental Fig. S2) of each sample was also recorded. The UV data showed that the fractionation patterns among the three fractions were distinct, and differences among stream water fractionation patterns were present within a site as well as among the sites (see also Supplemental

Fig. S2 for further details). The most pronounced difference was detected for Conventwald among the source Stream Point 1 and the remaining stream points and for Vessertal Stream Point 5 in comparison to the remaining Vessertal stream points. At Mitterfels, the fractionation pattern was very similar at all stream points, with a high first-fraction peak maximum relative to the second and third fractions. This was in line with minor changes between sample fractionation patterns at Wüstebach and Leirelva. Based on element concentrations from the AF^4 measurements (Fig. 2 shows example fractograms for Wüstebach Stream Point 7), the variability was estimated by comparing the concentrations in the fractions (Table 1). A high-intensity peak automatically corresponds to an elevated concentration in the respective fraction. Table 1 confirms the observed difference between Conventwald Stream Point 1 and the remaining Conventwald stream points (cf. Supplemental Fig. S2). On account of the element concentrations, the dominance of the first particle fraction at Mitterfels is evident only for organic C, while Fe shows similar high concentrations in the first and second fractions and Si clearly dominates in the third fraction. Further, at Wüstebach, the first fraction dominates in the sample from Stream Point 5, whereas peak concentrations in the second and third fractions were found in the sample from Stream Point 2. Similar comparisons of the fraction concentrations have been conducted by other researchers (Lyvén et al., 2003; Andersson et al., 2006; Stolpe et al., 2010; Regelink et al., 2013, 2014; Gottselig et al., 2014), yet clear trends of elemental concentrations in the patterns are not evident.

Dominant Phosphorus-Containing Colloid Size Fractions and Potential Phosphorus Carriers

To better assess the occurrence of the limiting nutrient P in the fractions, the size of the dominant P-containing fraction was determined. While colloidal P has been shown to contribute to plant P uptake (Montalvo et al., 2015), the uptake is assumed to vary in intensity depending on the P binding strength to NNP and colloids and thus P accessibility. The elemental fraction concentrations across five sites (Table 1) revealed a maximum P concentration in the third fraction of 13.55 μg L^{-1} in the source region of the Conventwald stream, indicating a high binding of P species to the clay-mineral-dominated fine colloid fraction. The highest P occurrence in the second fraction was detected for an overland-flow-driven tributary of the Wüstebach stream near the source area (Wüstebach Stream Point 2, 8.85 μg L^{-1} P), whereas the highest P in the first fraction was found for another overland-flow-driven tributary of the Wüstebach stream (Wüstebach Stream Point 5, 5.01 μg L^{-1} P). The overland-flow-driven tributaries are high in organic matter and potentially also Fe, two major components known to bind much P.

A comparison of the maximum concentrations of P per fraction and sample (bold type, Table 1) with the maximum concentrations of organic C, Al, Si, Mn, and Fe in the same samples per site (italic type, Table 1) showed a coincidence of maximum P concentrations with maximum concentrations of all other elements and organic C. In the first fraction of the samples from Wüstebach Stream Point 5 and Mitterfels Stream Point 3 as well as the second fraction from Mitterfels Stream Point 3 and the third fraction from Conventwald Stream Point 1, the maximum P coincides with the maximum concentration of all other elements and organic C. Specifically, organic C and/or Fe often peak when P concentrations are highest, yet an unequivocal assignment to a distinct carrier of P could not be done for the first and second fractions from a sole comparison of concentrations. To achieve this, improved data analysis techniques are necessary (see above). The sum of P concentrations in all of the third fractions of all of the samples is highest at 84.28 μg L^{-1}, followed by the second fraction at 58.24 μg L^{-1}, and the first fraction at 31.39 μg L^{-1} P (Table 1). This trend is confirmed by the average P per sample in each fraction (e.g., 84.28 μg L^{-1} P/29 samples = 2.91 μg L^{-1} P as the average per sample; c.f. Table 1), reflecting a high transport potential for P of the fine colloid fraction containing colloidal silica and clay minerals. This is possible either by direct adsorption of phosphate or by ligand exchange with metal (hydr)oxides associated with clay minerals as described above. Jiang et al. (2015) reported, though, that some P remained also bound to Fe-bearing phyllosilicate minerals after the extraction of Fe (hydr)oxides from soil fine colloids.

Association of Phosphorus with Natural Nanoparticles and Fine Colloids across Five Forest Streams: A Cluster Analysis Approach

To better understand the associations of P within the NNP and colloidal fractions, agglomerative hierarchical tree cluster analysis with complete linkage and the distance measure 1 − Pearson r was utilized to disentangle the potential associations of organic C, Fe, Al, Mn, and Si with P for each size fraction (Fig. 3). According to the results of this analysis, P clustered with Fe in the fraction 1 kDa to 20 nm, with a 1 − Pearson r distance of 0.16 (Fig. 3). This clustering supports the relevance of Fe (hydr)oxides, possibly in nanocrystalline form (Michel et al., 2007), for P binding in this smallest size fraction (Francko and Heath, 1982; Leppard et al., 1988; Hassellöv and von der Kammer, 2008; Jiang et al., 2015). The weak linkage of Al and P suggests that Al was not the major binding partner of P (Richardson, 1985) in this nanoparticle size. Phosphorus and organic C did not fall in the same cluster of this very fine nanoparticulate fraction. Organic C clustered more closely to Al and Mn than to Fe, suggesting that organic matter was mainly associated with these elements but questioning that organophosphorus compounds were the main component bound to the Fe oxides (Shafer et al., 1997; Lyvén et al., 2003; Regelink et al., 2011, 2013).

The analysis of the second fraction showed a different clustering. A close relation between P and organic C in the intermediate size fraction, covering particles >20 to 60 nm, was indicated. The

Table 1. Concentration of all elements in the three size fractions. Highlighted are maximum P concentrations per site (bold) and corresponding maximum concentrations of the other elements (italic).

Stream point	First fraction (1 kDa [0.66 nm]–20 nm)						Second fraction (>20–60 nm)						Third fraction (>60 nm)					
	OC†	Al	Si	P	Mn	Fe	OC	Al	Si	P	Mn	Fe	OC	Al	Si	P	Mn	Fe
	mg L⁻¹			µg L⁻¹			mg L⁻¹			µg L⁻¹			mg L⁻¹			µg L⁻¹		
Wüstebach																		
1	0.57	0.24	0.03	0.53	0.06	26.32	0.41	0.69	0.19	2.31	0.10	64.38	1.44	0.95	5.32	4.55	0.13	79.45
2	1.58	0.86	0.56	1.24	0.08	95.00	*1.85*	*3.19*	*5.11*	**8.85**	0.21	*291.79*	*3.56*	*2.25*	9.54	**8.64**	0.19	*213.16*
3	1.28	1.11	0.73	1.33	0.06	85.24	0.60	0.85	1.01	2.73	0.17	77.83	0.81	0.82	8.06	3.25	0.25	95.64
4	0.99	1.08	0.47	0.90	0.08	42.96	0.38	1.48	0.84	2.84	0.33	75.56	0.73	1.63	10.27	4.11	0.62	91.39
5	*4.42*	*5.14*	*2.28*	**5.01**	*0.24*	*138.93*	0.94	1.81	3.73	6.30	1.20	148.80	0.96	1.16	17.30	6.34	1.39	107.92
6	0.04	0.02	0.10	0.39	0.01	0.14	0.00	0.02	0.00	0.79	0.01	0.15	0.09	0.13	0.00	2.35	0.02	1.35
7	0.69	0.67	0.20	0.56	0.04	13.98	0.24	0.97	0.30	1.90	0.17	33.90	0.47	1.68	19.24	3.38	0.57	50.43
Vessertal																		
1	0.00	0.00	0.40	0.44	0.01	0.00	0.00	0.00	0.21	0.48	0.00	0.00	0.07	0.02	0.94	1.35	0.00	0.13
2	0.03	0.00	0.50	0.46	0.01	0.00	0.00	0.00	0.29	0.49	0.00	0.00	0.05	0.01	0.90	0.81	0.00	0.04
3	0.00	0.01	0.45	0.51	0.01	0.02	0.00	0.00	0.18	0.53	0.00	0.02	0.04	0.04	1.46	0.80	0.00	0.20
4	0.13	0.05	0.45	0.71	0.01	0.26	0.00	0.02	0.23	**0.82**	0.01	*0.14*	0.06	0.04	*1.06*	**1.75**	0.01	0.30
5	*0.13*	*0.07*	0.23	**0.74**	0.01	*0.58*	0.00	0.04	0.26	0.78	0.02	0.58	0.07	0.06	1.99	1.31	0.04	0.83
Mitterfels																		
1	4.98	2.99	1.61	1.62	0.20	28.45	0.75	2.09	2.99	2.56	0.19	23.79	0.30	0.46	7.19	2.39	0.08	8.37
2	4.17	2.94	1.02	1.49	0.13	26.47	0.53	1.90	1.57	2.15	0.15	20.27	0.22	0.44	6.31	2.53	0.09	8.17
3	*10.38*	*6.73*	*3.59*	**4.45**	*0.62*	*93.90*	*1.21*	*5.12*	*12.20*	**6.23**	*0.95*	*90.60*	*0.61*	*2.96*	23.58	**5.74**	*0.41*	*72.21*
4	3.19	3.04	2.41	1.35	0.19	23.07	0.45	1.99	3.60	2.59	0.23	21.66	0.30	2.42	48.67	2.59	0.22	23.02
5	4.49	4.57	2.59	1.86	0.24	32.90	0.55	3.28	5.52	3.49	0.34	32.97	0.32	2.26	39.30	3.01	0.25	27.55
6	3.35	5.36	2.55	1.69	0.12	32.51	0.53	3.46	5.60	2.95	0.38	32.82	0.36	1.56	14.86	2.23	0.65	28.99
7	3.28	4.43	2.08	1.35	0.05	27.79	0.48	2.37	3.74	2.25	0.13	22.14	0.35	2.01	30.38	2.16	0.25	21.58
8	1.85	2.74	1.06	0.97	0.06	17.78	0.29	1.94	1.77	1.83	0.25	18.46	0.25	1.71	19.89	2.45	0.53	28.30
Conventwald																		
1	0.05	0.37	7.50	0.54	0.09	1.98	0.00	0.00	0.00	0.61	0.08	0.61	*0.23*	*15.77*	*346.43*	**13.55**	*5.63*	*102.26*
2	*0.22*	0.09	0.31	**0.74**	0.01	0.51	0.00	0.03	0.05	0.82	0.01	0.27	0.05	0.11	3.24	2.25	0.02	0.77
3	0.06	0.01	0.50	0.26	0.01	0.10	0.00	0.01	0.23	0.26	0.00	0.03	0.04	0.04	1.37	0.19	0.01	0.29
4	0.07	0.03	0.45	0.45	0.01	0.16	0.00	0.01	0.17	0.53	0.00	0.05	0.05	0.06	1.94	1.37	0.02	0.37
5	0.05	0.03	0.39	0.23	0.00	0.39	0.00	*0.08*	*0.35*	**1.00**	0.04	*2.11*	0.05	0.21	4.08	2.04	0.09	3.61
Leirelva																		
1	0.70	0.04	0.19	0.39	0.06	2.34	0.09	0.04	0.00	0.57	0.05	1.43	0.35	0.00	0.75	0.77	0.06	1.00
2	*1.24*	*0.05*	0.00	**0.58**	0.06	*3.87*	*0.11*	0.03	0.00	**0.81**	0.05	*3.04*	0.31	0.02	4.88	1.16	0.10	3.06
3	0.68	0.04	0.07	0.23	0.07	2.91	0.07	0.04	0.02	0.36	0.06	2.16	0.31	0.01	0.04	0.47	0.05	1.28
4	0.61	0.03	0.50	0.37	0.07	2.84	0.05	0.02	0.05	0.41	0.06	1.82	0.27	0.01	0.53	**0.74**	0.06	1.26
Sum‡	49.23	42.74	33.22	31.39	2.61	701.40	9.53	31.48	50.21	58.24	5.19	967.38	12.72	38.84	629.52	84.28	11.74	972.93
Avg.§	1.70	1.47	1.15	1.08	0.09	24.19	0.33	1.09	1.73	2.01	0.18	33.36	0.44	1.34	21.71	2.91	0.40	33.55

† OC, organic carbon.
‡ Sum indicates the concentration sum of the corresponding column.
§ Average is the sum concentration divided by 29 samples.

further clustering of P and organic C with Fe may indicate an association of Fe to one or both of these elements, which would support the assumption that this fraction consisted of organic matter bound to Fe and of Fe to P through ligand exchange (Gerke, 1992; Gerke and Hermann, 1992) or of organophosphorus compounds associated with Fe (hydr)oxides (Gerke, 1992, 2015). The association of organophosphorus with Fe (hydr)oxides is more likely if following the cluster analysis results.
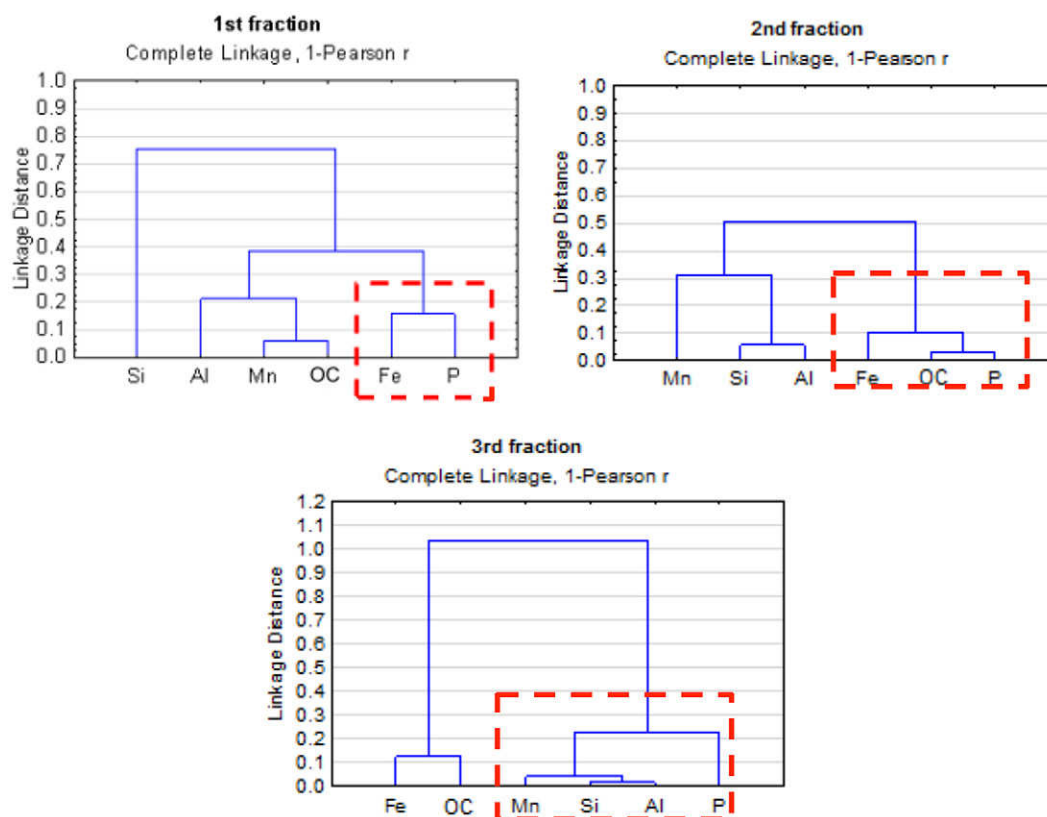
Fig. 3. Hierarchical tree cluster analysis with 1 − Pearson's *r* as the distance measure and complete linkage rule per fraction across all sampling sites. The height of the boxes equals the 1 − Pearson's *r* distance. A low value of the linkage distance indicates stronger potential binding. The dotted squares show the major binding partners of P in the natural nanoparticle and fine colloidal fractions.

According to the results of the cluster analysis, P in the third fraction strongly associated with Al, Si, and Mn rather than Fe and/or organic C. The distance measure of Si to Al is very small (1 − Pearson r = 0.02), reflecting a common compound, such as phyllosilicates. Indeed, phyllosilicates may contain variable amounts of other elements (Grim and Kodama, 2014). The clustering of Mn with Si and Al specifically points to the potential presence of 2:1 clay minerals. In expansive 2:1 clays, which can take up nutrients and water, Al can be replaced by Fe or Mn. Apparently, in this fraction, P was sorbed to the surfaces of clay minerals by ligand exchange with a metal hydroxide (Yaghi and Hartikainen, 2013). In any case, the analyses clearly show that NNP and fine colloids of forest stream waters not only differed in hydrodynamic diameter but also in their composition, thus rendering the complex and important carriers for colloidal P and other elements of different binding form and possibly origin.

A comparison with other studies reveals that the differentiation of multiple size classes within the natural nanoparticles and fine colloids is rarely reported in combination with P sorption. Different numbers of particle size fractions separated by the FFF technique seem to be present in different environmental samples (Stolpe et al., 2010; Regelink et al., 2011, 2013). In the latter studies, the smaller size range was assigned to organic matter associated with metal oxides and the larger fraction (up to 100 nm) to clay or colloidal

silica. The present study implies an associated transport of P and clay minerals in the largest size fraction when particles exceed a hydrodynamic diameter of 60 nm.

Potential Ecological Relevance of Natural Nanoparticles and Fine Colloids in Forest Stream Waters

A high relevance of NNP and fine colloids for nutrient cycling in ecosystems is indicated by the high percentages of essential element binding (especially organic C, Mn, Fe, and P) to the NNP and fine colloidal fractions (Table 2; Supplemental Table S2). Up to 100% of elements were bound to NNP and colloids. The difference between total sample concentration and particulate concentration could potentially be assigned to the dissolved fraction (Martin et al., 1995; Hill and Aplin, 2001) as simply hydrated compounds <1 kDa. We note that the interdependency of the colloidal and nanoparticulate fractions with the dissolved phase is less known.

The percentage of organic C and Mn associated with NNP and fine colloids varied among sites from 7 to 50 and 15 to 80%, respectively. These elements did not vary in a comparative way, indicating that different factors affect organic C and Mn concentrations in stream waters. Large organic matter inputs can be expected for thick and highly developed organic soil horizons, whereas Mn, as an important redox element for multiple biological processes, can

indicate microbial activity and turnover (Keiluweit et al., 2015). The percentages of Fe associated with NNP and fine colloids ranged from 26 to 57% and were intermediate and less variable than other observed elements. In contrast, total Fe concentrations varied more and significantly. Hence, Fe binding to NNP and fine colloids appears to be a favorable and stable process that declines only when Fe is present in very low concentrations. Aluminum and Si were detected in high amounts in the total sample, yet the percentage of Al bound to NNP and fine colloids was generally <5%, for Si even <2% (cf. Supplemental Table S2), probably reflecting the acidic conditions of the ecosystems. Larger sample sizes across various ecosystems, preferably at a continental scale, are now needed to relate these patterns to the properties of the streams (water chemistry, flow rate, temperature) or ecosystems (climate, geology, vegetation stands).

Noteworthy, the contribution of NNP and fine colloids as carriers for P increased with decreasing total P concentration: total P concentration and the percentage of P binding in the three fractions (Table 3) were negatively correlated, i.e., either the NNP and colloids were P saturated so that they could not take up additional P when total P concentrations increased, or dissolved P did not come in close contact with these particles during stream transport to allow a binding to these fractions. Overall, the P-containing particles thus constitute a high relevance for nutrient cycling or similarly represent a major loss factor, which is of high expense to the ecosystem (Bol et al., 2016).

◉ Conclusion

This study showed that P binding to the NNP and fine colloidal fractions of stream waters is not restricted to a single particle type but that there is a size-dependent binding of P to different organic, inorganic, and/or mineral constituents. The successful coupling of FFF to OCD and ICP–MS revealed three main fractions of these nanoparticles and fine colloids. The primary associations of P were to small nanosized Fe oxides, while in the nanoparticulate medium-sized fraction, P binding was increasingly affected also by the presence of organic matter. Finally, clay minerals were involved in the P association in larger nanoparticles to fine colloids. Moreover, an increasing percentage of P is associated with NNP and fine colloids, especially as the total P concentration declines. Our results demonstrate that NNP and fine colloids play a relevant role for nutrient transport in and export from forest ecosystems.

Table 2. Phosphorus fractionation in stream water samples: particle fractionation via asymmetric flow field flow fractionation coupled online to inductively couple plasma–mass spectrometry and organic C detection, and the binding percentage of P per nanoparticulate and fine colloidal fraction related to total P concentration as well as their sum across all stream points per site.

Stream point	P binding per fraction†				Total P‡	Particulate P§
	First	Second	Third	$\sum$		
	——————% ——————				—————— L^{-1} ——————	
Conventwald						
1	1.3	1.5	33.9	36.7	40.0	14.7
2	2.6	2.9	8.0	13.6	28.0	3.8
3	1.9	1.8	1.3	5.1	14.0	0.7
4	3.3	3.9	10.1	17.3	13.6	2.3
5	2.3	9.9	20.2	32.3	10.1	3.3
Mitterfels						
1	7.0	11.1	10.4	28.6	23.0	6.6
2	5.5	8.0	9.4	22.9	27.0	6.2
3	7.8	10.9	10.1	28.8	57.0	16.4
4	9.0	17.2	17.3	43.5	15.0	6.5
5	9.0	16.9	14.6	40.6	20.6	8.4
6	12.1	21.1	15.9	49.1	14.0	6.9
7	10.4	17.3	16.6	44.3	13.0	5.8
8	5.1	9.6	12.9	27.7	19.0	5.3
Vessertal						
1	4.2	4.6	13.0	21.8	10.4	2.3
2	2.2	2.3	3.9	8.4	21.0	1.8
3	1.4	1.4	2.2	5.0	37.0	1.8
4	4.4	5.1	10.9	20.5	16.0	3.3
5	6.7	7.1	11.9	25.8	11.0	2.8
Wüstebach						
1	5.1	22.4	44.1	71.7	10.3	7.4
2	5.4	38.5	37.6	81.4	23.0	18.7
3	14.8	30.3	36.1	81.2	9.0	7.3
4	10.0	31.6	45.7	87.3	9.0	7.9
5	26.4	33.1	33.4	92.9	19.0	17.6
6	2.8	5.6	16.7	25.1	14.1	3.5
7	8.1	27.5	48.9	84.5	6.9	5.8
Leirelva						
1	18.7	29.2	42.6	90.5	1.5	1.4
2	20.2	28.4	40.3	88.9	1.3	1.2
3	19.1	30.2	39.3	88.5	1.2	1.1
4	15.4	33.5	38.4	87.3	0.9	0.8

† First fraction, >1 kDa–20 nm; second fraction, >20–60 nm; third fraction, >60 nm.
‡ Total sample P concentration.
§ Sum of P concentration across all three fractions ($n = 29$).

Table 3. The correlation coefficients between the total elemental concentrations and the percentages of particle-bound element concentrations. Coefficients were calculated according to Spearman r correlation.

Fraction	Correlation of total elemental concentration to particle-bound concentration percentage					
	P	Organic C	Al	Si	Mn	Fe
First	−0.52*	0.58*	0.22	−0.25	−0.66*	−0.05
Second	−0.54*	0.73*	0.39*	−0.27	−0.52*	0.37*
Third	−0.66*	−0.36	0.06	−0.31	−0.60*	−0.12
All	−0.56*	0.58*	0.29	−0.25	−0.56*	0.08

* Significant correlation at $p < 0.05$.

The hyphenated AF[4] analysis can contribute to a better understanding of soil evolution and formation mechanisms.

References

Andersson, K., R. Dahlqvist, D. Turner, B. Stolpe, T. Larsson, J. Ingri, and P. Andersson. 2006. Colloidal rare earth elements in a boreal river: Changing sources and distributions during the spring flood. Geochim. Cosmochim. Acta 70:3261–3274. doi:10.1016/j.gca.2006.04.021

Baalousha, M., B. Stolpe, and J.R. Lead. 2011. Flow field-flow fractionation for the analysis and characterization of natural colloids and manufactured nanoparticles in environmental systems: A critical review. J. Chromatogr. A 1218:4078–4103. doi:10.1016/j.chroma.2011.04.063

Binkley, D., G.G. Ice, J. Kaye, and C.A. Williams. 2004. Nitrogen and phosphorus concentrations in forest streams of the United States. J. Am. Water Resour. Assoc. 40:1277–1291. doi:10.1111/j.1752-1688.2004.tb01586.x

Bol, R., D. Julich, D. Brödlin, J. Siemens, K. Kaiser, M.A. Dippold, et al. 2016. Dissolved and colloidal phosphorus fluxes in forest ecosystems: An almost blind spot in ecosystem research. J. Plant Nutr. Soil Sci. 179:425–438. doi:10.1002/jpln.201600079

Climatemps. 2014. Trondheim climate and temperature. http://www.trondheim.climatemps.com/ (accessed 3 Nov. 2014)

Crini, G., and P.M. Badot. 2010. Sorption processes and pollution: Conventional and non-conventional sorbents for pollutant removal from wastewaters. Presses Universitaires de Franche-Comté, Besançon, France.

Dahlqvist, R., M.F. Benedetti, K. Andersson, D. Turner, T. Larsson, B. Stolpe, and J. Ingri. 2004. Association of calcium with colloidal particles and speciation of calcium in the Kalix and Amazon rivers. Geochim. Cosmochim. Acta 68:4059–4075. doi:10.1016/j.gca.2004.04.007

Darch, T., M.S.A. Blackwell, J.M.B. Hawkins, P.M. Haygarth, and D. Chadwick. 2014. A meta-analysis of organic and inorganic phosphorus in organic fertilizers, soils, and water: Implications for water quality. Crit. Rev. Environ. Sci. Technol. 44:2172–2202. doi:10.1080/10643389.2013.790752

Edzwald, J.K., D.C. Toensing, and M.C.-Y. Leung. 1976. Phosphate adsorption reactions with clay minerals. Environ. Sci. Technol. 10:485–490. doi:10.1021/es60116a001

Erickson, H.P. 2009. Size and shape of protein molecules at the nanometer level determined by sedimentation, gel filtration, and electron microscopy. Biol. Proced. Online 11:32–51. doi:10.1007/s12575-009-9008-x

Filella, M., C. Deville, V. Chanudet, and D. Vignati. 2006. Variability of the colloidal molybdate reactive phosphorous concentrations in freshwaters. Water Res. 40:3185–3192. doi:10.1016/j.watres.2006.07.010

Francko, D.A., and R.T. Heath. 1982. UV-sensitive complex phosphorus: Association with dissolved humic material and iron in a bog lake. Limnol. Oceanogr. 27:564–569. doi:10.4319/lo.1982.27.3.0564

Franco, A., W.J. Fu, and S. Trapp. 2009. Influence of soil pH on the sorption of ionizable chemicals: Modelling advances. Environ. Toxicol. Chem. 28:458–464. doi:10.1897/08-178.1

Gerke, J. 1992. Orthophosphate and organic phosphate in the soil solution of four sandy soils in relation to pH-evidence for humic–Fe–(Al–) phosphate complexes. Commun. Soil Sci. Plant Anal. 23:601–612. doi:10.1080/00103629209368612

Gerke, J. 2015. The acquisition of phosphate by higher plants: Effect of carboxylate release by the roots: A critical review. J. Plant Nutr. Soil Sci. 178:351–364. doi:10.1002/jpln.201400590

Gerke, J., and R. Hermann. 1992. Adsorption of orthophosphate to humic-Fe-complexes and to amorphous Fe-oxide. Z. Pflanzenernaehr. Bodenkd. 155:233–236. doi:10.1002/jpln.19921550313

Giddings, J., F. Yang, and M. Myers. 1976. Flow-field-flow fractionation: A versatile new separation method. Science 193:1244–1245. doi:10.1126/science.959835

Gimbert, L.J., K.N. Andrew, P.M. Haygarth, and P.J. Worsfold. 2003. Environmental applications of flow field-flow fractionation (FIFFF). TrAC, Trends Anal. Chem. 22:615–642. doi:10.1016/S0165-9936(03)01103-8

Gottselig, N., R. Bol, V. Nischwitz, H. Vereecken, W. Amelung, and E. Klumpp. 2014. Distribution of phosphorus-containing fine colloids and nanoparticles in stream water of a forest catchment. Vadose Zone J. 13(7). doi:10.2136/vzj2014.01.0005

Greenberg, A. 1985. Standard methods for the examination of water and wastewater. 16th ed. Am. Public Health Assoc., Washington, DC.

Grim, R., and H. Kodama. 2014. Clay mineral. In: Encyclopedia Britannica. Encyclopædia Britannica Inc., Chicago.

Hartland, A., J.R. Lead, V. Slaveykova, D. O'Carroll, and E. Valsami-Jones. 2013. The environmental significance of natural nanoparticles. Nat. Educ. Knowl. 4(8):7.

Hassellöv, M., B. Lyvén, C. Haraldsson, and W. Sirinawin. 1999. Determination of continuous size and trace element distribution of colloidal material in natural water by on-line coupling of flow field-flow fractionation with ICPMS. Anal. Chem. 71:3497–3502. doi:10.1021/ac981455y

Hassellöv, M., and F. von der Kammer. 2008. Iron oxides as geochemical nanovectors for metal transport in soil–river systems. Elements 4:401–406. doi:10.2113/gselements.4.6.401

Heathwaite, A.L., and R.M. Dils. 2000. Characterising phosphorus loss in surface and subsurface hydrological pathways. Sci. Total Environ. 251–252:523–538. doi:10.1016/S0048-9697(00)00393-4

Hill, D.M., and A.C. Aplin. 2001. Role of colloids and fine particles in the transport of metals in rivers draining carbonate and silicate terrains. Limnol. Oceanogr. 46:331–344. doi:10.4319/lo.2001.46.2.0331

Huber, S.A., A. Balz, M. Abert, and W. Pronk. 2011. Characterisation of aquatic humic and non-humic matter with size-exclusion chromatography: Organic carbon detection–organic nitrogen detection (LC-OCD-OND). Water Res. 45:879–885. doi:10.1016/j.watres.2010.09.023

Huber, S.A., and F.H. Frimmel. 1991. Flow injection analysis of organic and inorganic carbon in the low-ppb range. Anal. Chem. 63:2122–2130. doi:10.1021/ac00019a011

Jarvie, H.P., C. Neal, A.P. Rowland, M. Neal, P.N. Morris, J.R. Lead, et al. 2012. Role of riverine colloids in macronutrient and metal partitioning and transport, along an upland–lowland land-use continuum, under low-flow conditions. Sci. Total Environ. 434:171–185. doi:10.1016/j.scitotenv.2011.11.061

Jiang, X., R. Bol, V. Nischwitz, N. Siebers, S. Willbold, H. Vereecken, et al. 2015. Phosphorus containing water dispersible nanoparticles in arable soil. J. Environ. Qual. 44:1772–1781. doi:10.2134/jeq2015.02.0085

Keiluweit, M., P. Nico, M.E. Harmon, J. Mao, J. Pett-Ridge, and M. Kleber. 2015. Long-term litter decomposition controlled by manganese redox cycling. Proc. Natl. Acad. Sci.112:E5253–E5260. doi:10.1073/pnas.1508945112

Klitzke, S., and F. Lang. 2007. Hydrophobicity of soil colloids and heavy metal mobilization: Effects of drying. J. Environ. Qual. 36:1187–1193. doi:10.2134/jeq2006.0427

Leppard, G.G., J. Buffle, R.R. Devitre, and D. Perret. 1988. The ultrastructure and physical characteristics of a distinctive colloidal iron particulate isolated from a small eutrophic lake. Arch. Hydrobiol. 113:405–424.

Liski, J., D. Perruchoud, and T. Karjalainen. 2002. Increasing carbon stocks in the forest soils of Western Europe. For. Ecol. Manage. 169:159–175. doi:10.1016/S0378-1127(02)00306-7

Liu, J., X. Liang, J. Yang, Y. Ye, M. Su, Z. Nie, and Y. Chen. 2011. Size distribution and composition of phosphorus in the East Tiao River, China: The significant role of colloids. J. Environ. Monit. 13:2844–2850. doi:10.1039/c1em10482a

Lyvén, B., M. Hassellöv, D.R. Turner, C. Haraldsson, and K. Andersson. 2003. Competition between iron- and carbon-based colloidal carriers for trace metals in a freshwater assessed using flow field-flow fractionation coupled to ICPMS. Geochim. Cosmochim. Acta 67:3791–3802. doi:10.1016/S0016-7037(03)00087-5

Martin, J.M., M.H. Dai, and G. Cauwet. 1995. Significance of colloids in the biogeochemical cycling of organic carbon and trace metals in the Venice Lagoon (Italy). Limnol. Oceanogr. 40:119–131. doi:10.4319/lo.1995.40.1.0119

Mayer, T.D., and W.M. Jarrell. 1995. Assessing colloidal forms of phosphorus and iron in the Tualatin-River basin. J. Environ. Qual. 24:1117–1124. doi:10.2134/jeq1995.00472425002400060010x

Michel, F.M., L. Ehm, S.M. Antao, P.L. Lee, P.J. Chupas, G. Liu, et al. 2007. The structure of ferrihydrite, a nanocrystalline material. Science 316:1726–1729. doi:10.1126/science.1142525

Montalvo, D., F. Degryse, and M.J. McLaughlin. 2015. Natural colloidal P and its contribution to plant P uptake. Environ. Sci. Technol. 49:3427–3434. doi:10.1021/es504643f

Neubauer E., F.v.d. Kammer, and T. Hofmann. 2013. Using FlowFFF and HPSEC to determine trace metal colloid associations in wetland runoff. Water Res. 47:2757–2769. doi:10.1016/j.watres.2013.02.030

Nischwitz, V., and H. Goenaga-Infante. 2012. Improved sample preparation and quality control for the characterisation of titanium dioxide nanoparticles in sunscreens using flow field flow fractionation on-line with inductively coupled plasma mass spectrometry. J. Anal. At. Spectrom. 27:1084–1092. doi:10.1039/c2ja10387g

Owens, L.B., and M.J. Shipitalo. 2006. Surface and subsurface phosphorus losses from fertilized pasture systems in Ohio. J. Environ. Qual. 35:1101–1109. doi:10.2134/jeq2005.0402

Qafoku, N.P. 2010. Terrestrial nanoparticles and their controls on soil-/geo-processes and reactions. Adv. Agron. 107:33–91. doi:10.1016/S0065-2113(10)07002-1

Ranville, J.F., and D.L. Macalady. 1997. Natural organic matter in catchments. In: O.M. Sather and P. de Caritat, editors, Geochemical processes, weathering and groundwater recharge in catchments. A.A. Balkema, Rotterdam, the Netherlands.

Reddy, K.R., O.A. Diaz, L.J. Scinto, and M. Agami. 1995. Phosphorus dynamics in selected wetlands and streams of the Lake Okeechobee basin. Ecol. Eng. 5:183–207.

Regelink, I.C., G.F. Koopmans, C. van der Salm, L. Weng, and W.H. van Riemsdijk. 2013. Characterization of colloidal phosphorus species in drainage waters from a clay soil using asymmetric flow field-flow fractionation. J. Environ. Qual. 42:464–473. doi:10.2134/jeq2012.0322

Regelink, I.C., A. Voegelin, L.P. Weng, G.F. Koopmans, and R.N.J. Comans. 2014. Characterization of colloidal Fe from soils using field-flow fractionation and Fe K-edge X-ray absorption spectroscopy. Environ. Sci. Technol. 48:4307–4316. doi:10.1021/es405330x

Regelink, I.C., L. Weng, and W.H. van Riemsdijk. 2011. The contribution of organic and mineral colloidal nanoparticles to element transport in a podzol soil. Appl. Geochem. 26:S241–S244. doi:10.1016/j.apgeochem.2011.03.114

Reszat, T.N., and M.J. Hendry. 2005. Characterizing dissolved organic carbon using asymmetrical flow field-flow fractionation with on-line UV and DOC detection. Anal. Chem. 77:4194–4200. doi:10.1021/ac048295c

Richardson, C.J. 1985. Mechanisms controlling phosphorus retention capacity in fresh-water wetlands. Science 228:1424–1427. doi:10.1126/science.228.4706.1424

Schmitt, D., H.E. Taylor, G.R. Aiken, D.A. Roth, and F.H. Frimmel. 2002. Influence of natural organic matter on the adsorption of metal ions onto clay minerals. Environ. Sci. Technol. 36:2932–2938. doi:10.1021/es010271p

Shafer, M.M., J.T. Overdier, J.P. Hurley, D. Armstrong, and D. Webb. 1997. The influence of dissolved organic carbon, suspended particulates, and hydrology on the concentration, partitioning and variability of trace metals in two contrasting Wisconsin watersheds (USA). Chem. Geol. 136:71–97. doi:10.1016/S0009-2541(96)00139-8

Spivakov, B.Y., T.A. Maryutina, and H. Muntau. 2009. Phosphorus speciation in water and sediments. Pure Appl. Chem. 71:2161–2176.

Stolpe, B., L. Guo, A.M. Shiller, and M. Hassellöv. 2010. Size and composition of colloidal organic matter and trace elements in the Mississippi River, Pearl River and the northern Gulf of Mexico, as characterized by flow field-flow fractionation. Mar. Chem. 118:119–128. doi:10.1016/j.marchem.2009.11.007

Stolpe, B., and M. Hassellöv. 2007. Changes in size distribution of fresh water nanoscale colloidal matter and associated elements on mixing with seawater. Geochim. Cosmochim. Acta 71:3292–3301. doi:10.1016/j.gca.2007.04.025

Stolpe, B., M. Hassellöv, K. Andersson, and D.R. Turner. 2005. High resolution ICPMS as an on-line detector for flow field-flow fractionation: Multi-element determination of colloidal size distributions in a natural water sample. Anal. Chim. Acta 535:109–121. doi:10.1016/j.aca.2004.11.067

Wilkinson, K.J., A. Joz-Roland, and J. Buffle. 1997. Different roles of pedogenic fulvic acids and aquagenic biopolymers on colloid aggregation and stability in freshwaters. Limnol. Oceanogr. 42:1714–1724. doi:10.4319/lo.1997.42.8.1714

Yaghi, N., and H. Hartikainen. 2013. Enhancement of phosphorus sorption onto light expanded clay aggregates by means of aluminum and iron oxide coatings. Chemosphere 93:1879–1886. [erratum: 103:359] doi:10.1016/j.chemosphere.2013.06.059

Zirkler, D., F. Lang, and M. Kaupenjohann. 2012. "Lost in filtration": The separation of soil colloids from larger particles. Colloids Surf. A 399:35–40. doi:10.1016/j.colsurfa.2012.02.021